Aerodynamic Characteristics of the Planetary Atmosphere Experiments Test Entry Probe

ROBERT I. SAMMONDS* AND ROBERT L. KRUSE*
NASA Ames Research Center, Moffett Field, Calif.

The aerodynamic characteristics of the PAET entry probe were determined experimentally in ballistic range tests over a wide range of Mach and Reynolds numbers, and compared with full-scale flight results. The ground facility data agreed with the full-scale data within 2 to 3% in drag coefficient, and within 5 to 10% in static stability, at the higher Mach numbers. Comparisons of the flight data with conventional wind tunnel data indicated a significant disagreement in drag coefficient in the transonic speed range suggestive of important sting or wall interference effects. Variations in drag coefficient with Mach number were very small hypersonically, but variations with Reynolds number were of the order of 15% at $M_\infty = 13$ over the Reynolds number range of 10^4 to 10^6. Variations in the lift and static-stability curves with Mach number and Reynolds number were also defined.

Nomenclature

A = reference area, maximum body cross-sectional area, m^2
C_D = drag coefficient, drag/$q_\infty A$
C_L = lift coefficient, lift/$q_\infty A$
C_{L_α} = lift-curve slope, per rad
C_m = pitching-moment coefficient, moment/$q_\infty Ad$
C_{m_α} = pitching-moment-curve slope (based on an assumed linear pitching-moment curve), per rad
$C_{m_q}+C_{m_{\dot\alpha}}$ = damping-in-pitch derivative, $\partial C_m/\partial(qd/V)+\partial C_m/\partial(\dot\alpha d/V)$, per rad
d = reference diameter, maximum body diameter, m
I_x = moment of inertia about the roll axis, kg-m^2
I_y = moment of inertia about a transverse axis through center of gravity, kg-m^2
M = Mach number
m = mass of model, kg
q = angular pitching velocity, rad/sec
q_∞ = freestream dynamic pressure, N/m^2
Re_d = Reynolds number based on freestream air properties and model reference diameter
r = radius of curvature, cone apex or base, m
V = velocity of model with respect to still air, km/sec
X_{cg}, X_{cp} = axial distance from model nose to center of gravity and center of pressure, respectively, m
x,y,z = Earth-fixed axes; also displacements along these axes, m
y,z dev = rms deviation of measured lateral position coordinates of model in free flight from curves fitted to the data, cm
α = angle of attack (angle, projected onto the xz plane, between model longitudinal axis and the velocity vector), deg
$\alpha_m, \alpha_{\min}$ = average value of maximum and minimum angle-of-attack envelope, respectively, deg
$\alpha_{\rm rms}$ = rms resultant angle of attack, $\left(\frac{\int_0^x \alpha_r^2\,dx}{x}\right)^{1/2}$, deg
α_r = resultant angle of attack, $(\alpha^2+\beta^2)^{1/2}$, deg
β = angle of sideslip (angle, projected onto the xy plane, between model axis of symmetry and the velocity vector), deg
$\alpha, \beta_{\rm dev}$ = rms deviation of measured angles of attack and sideslip of model in free flight from curves fitted to the data, deg
ρ = freestream air density, kg/m^3
$(\dot{})$ = first derivative with respect to time

Subscripts
b = base
n = nose
∞ = freestream

Received March 26, 1974; revision received September 9, 1974.
Index categories: Entry Vehicle Dynamics and Control; Entry Vehicles and Landers.
* Research Scientist. Member AIAA.

Introduction

THE determination of the structure of unknown planetary atmospheres by means of unmanned instrumented entry probes [1-3] can be based on on-board measurements of acceleration, pressure, and temperature in appropriate phases of the entry. The validity of this technique was proven with the flight of the PAET (Planetary Atmosphere Experiments Test) vehicle in the Earth's atmosphere on June 20, 1971.[4]

To reconstruct the atmosphere from these data requires that the vehicle have known and well-defined aerodynamic characteristics (drag coefficient in particular) and be aerodynamically stable to ensure the proper orientation of the heat shield and the pressure and temperature sensors. In support of the PAET experiments, an investigation was conducted in still air in the NASA Ames Research Center Hypervelocity Free-Flight Aerodynamics Facility[5] to determine the aerodynamic characteristics of the PAET vehicle over the range of Mach numbers, Reynolds numbers, and angles of attack that would be encountered during the entry. The results of that investigation are presented here.

Although the concept of PAET was to validate the technique for measuring a planetary atmosphere, the simultaneous measurement of the Earth's atmosphere by means of Radiosondes, Arcasondes, and Viper Dart inflated spheres[4] presented a unique opportunity to study this experiment instead as an extremely well-instrumented, full-scale test to define the aerodynamic characteristics of the entry probe. As such, comparisons are presented here between the full-scale flight data, certain previous data obtained in the Ames ballistic facilities,[6,7] and the present data. Included in this comparison are comparable wind-tunnel data[8-15] and unpublished data from the Ames 1- by 3- and 2- by 2-ft Wind Tunnels.

Models

The configuration tested closely duplicated the PAET shape (Fig. 1a) which consisted of a 55° half-angle, spherically blunted cone with a spherical segment afterbody. The ratio of nose to base radius (r_n/r_b) was 1.0 and the spherical segment afterbody had its center of curvature located at a point 0.20 diameter aft of the model nose, coincident with the center of gravity of the flight vehicle and the basic test model. However, for some tests,

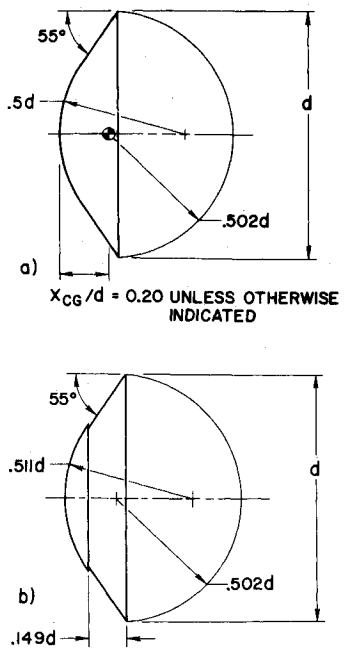

Fig. 1 PAET test configurations; a) basic configuration, b) basic configuration with upset face.

an externally identical, homogeneous model also was used and its center of gravity was 0.34 diameter aft of the nose. The forward center-of-gravity location was obtained by ballast. To evaluate the effect on the aerodynamic characteristics of a possible discontinuity between the beryllium heat shield on the PAET vehicle and the ablative heat shield, some models (Fig. 1b) were tested with an upset face, and a spherical nose radius increased from 0.50 to 0.511d to produce the discontinuity shown.

Tests

The models were tested in free flight in still air in the Ames Hypervelocity Free-Flight Aerodynamic Facility over a range of Mach numbers and Reynolds numbers shown in Table 1. The angles of attack ranged from 0° to 40°. This range of test conditions is comparable to those experienced by the PAET vehicle during its entry into the Earth's atmosphere. Tabulated summaries of the actual test conditions and the principal results may be obtained from the authors. The models were launched from 38.1 (1.5 in.), 25.4 (1 in.), and 12.7 (0.5 in.) mm diam deformable piston, light-gas guns.[16] The models were adapted to the guns by means of four-piece polycarbonate plastic (Lexan) sabots.

Table 1 Range of data for free-flight tests

M_∞	$Re_d \times 10^{-6}$
0.8 to 8.9	0.5 to 1.7
13.0	0.005 to 0.7

Instrumentation

Shadowgraphs of the models were obtained in orthogonal planes at 16 evenly spaced observation stations over a ballistic flight of 23 m (75 ft). Each photographic observation station contained calibrated fiducial references so that the spatial position and attitude of the model could be determined accurately. Electronic chronographs were used to measure the time of model flight between stations.

Accuracy of Data

The accuracies of the measured quantities used to obtain the aerodynamic coefficients from the model motions are shown in Table 2.

Table 2 Accuracies of the measured quantities

Measurement	*Accuracy*
x, y, z	± 0.013 cm
α, β	$\pm 0.25°$
t	± 0.02 μsec
p_∞	± 0.1 mm Hg above 10 mm ± 0.05 mm Hg below 10 mm

Data Reduction

To determine the aerodynamic characteristics of the configurations tested, their free-flight motions were analyzed using the data reduction program described in Ref. 17. This program determines drag from the time-distance history of each flight, static and dynamic stability from the oscillatory history of the model, and lift-curve slope from the swerve measurements and oscillatory motion of the model, under the assumption of linear aerodynamics. The data thus obtained over a range of motion amplitudes were interpreted to define nonlinear lift and stability coefficients by methods described in Refs. 17–19.

Results and Discussion

The aerodynamic coefficients and the center of pressure obtained for the PAET entry configuration are given in Figs. 2–8. A comparison of these data with data for a comparable model with a simulated heat-shield discontinuity is presented in Fig. 9. Figure 10 shows the Reynolds number and angle-of-attack history for the full-scale vehicle during re-entry as a function of Mach number, while Figs. 11 and 12 show comparisons of drag and static stability coefficients, respectively, between the full-scale vehicle and ground-based facilities (ballistic range and wind tunnels).

Drag Coefficient

Drag coefficient data are presented in Fig. 2 for the complete test range. These data (Figs. 2a–c) show that C_D decreases with

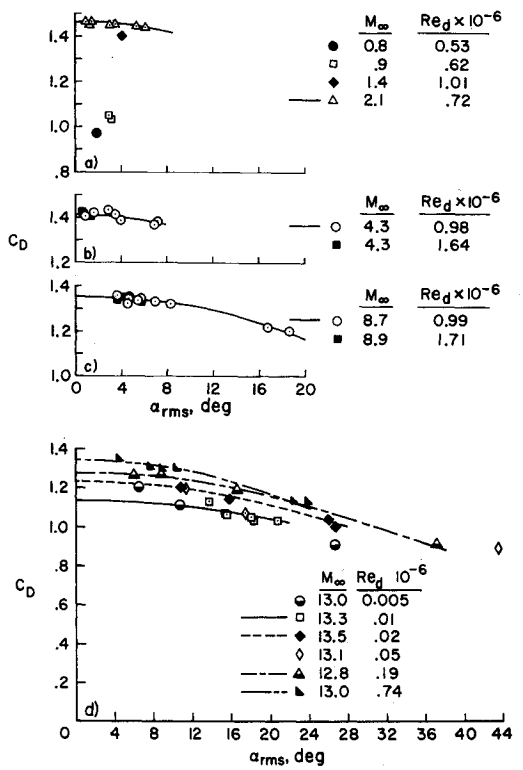

Fig. 2 Variation of drag coefficient with angle of attack; a) $0.8 \leq M_\infty \leq 2.1$, b) $M_\infty \approx 4.3$, c) $M_\infty \approx 8.8$, and d) $M_\infty \approx 13$.

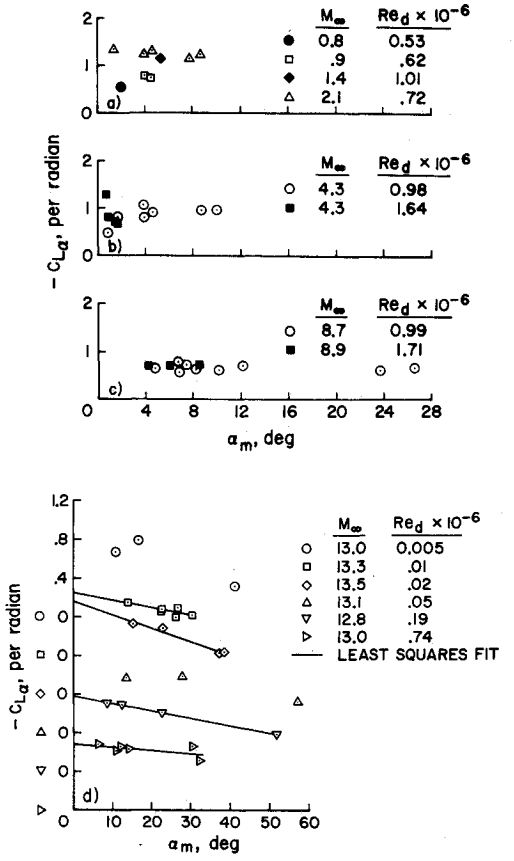

Fig. 3 Variation of lift-curve slope with pitch amplitude; a) $0.8 < M_\infty < 2.1$, b) $M_\infty \approx 4.3$, c) $M_\infty \approx 8.8$, and d) $M_\infty \approx 13$.

both increasing M_∞ and angle of attack for $M_\infty > 2$. The data show also (Fig. 2d) that, for $M_\infty = 13$, C_D decreases significantly with decreasing Reynolds number, particularly for R_{e_d} below 50,000. (Note that curves have not been faired through the 5000, 50,000 Re_d data because the limited number of points is not sufficient to adequately define the shape of these curves.)

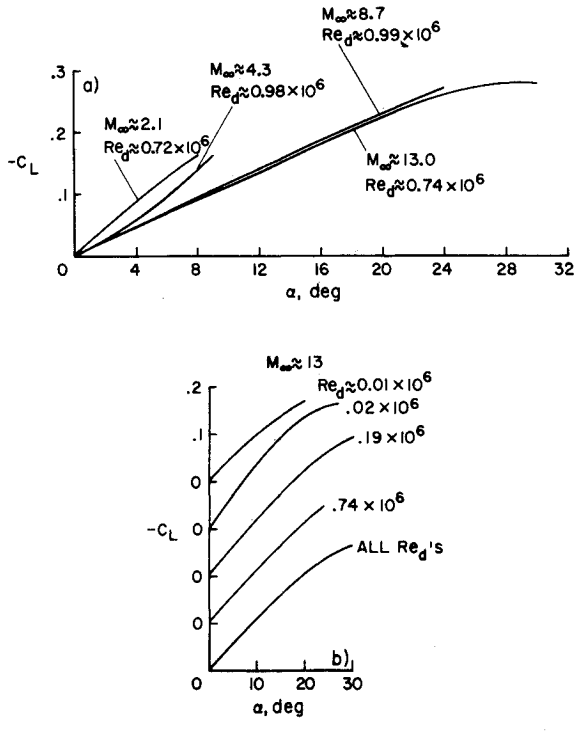

Fig. 4 Lift coefficient vs angle-of-attack; a) $2.1 < M_\infty < 13$, and b) $M_\infty \approx 13$.

Lift Coefficient

The quasilinear lift-curve slopes and the nonlinear lift curves derived from them are presented in Figs. 3 and 4, respectively. The lift-curve slopes are negative, as is typical of large-angled blunt bodies, decreasing rapidly as M_∞ increases from 2–9 but are nearly unchanged from 9–13. Near linearity is shown in C_{L_z} for the lower Mach numbers (<9) and higher Reynolds numbers ($\approx 10^6$) by nearly constant values of C_{L_z} obtained at all amplitudes of oscillation. In contrast, the lift-curve slopes obtained at $M_\infty = 13$ show evidence of decreasing slope with increasing pitch amplitude (Fig. 3d), with the rate of decrease depending on the Reynolds number. Least square fits of straight lines to the data define the rates of decrease of C_{L_z} with increasing amplitude. Nonlinear lift curves derived from these data are presented in Fig. 4. At the higher Reynolds numbers, $C_L(\alpha)$ decreases with increasing Mach number. At $M_\infty = 13$, decreasing Reynolds number seems to increase nonlinearity (Fig. 4b) except for a $Re_d = 10^4$, where the trend appears to be reversed.

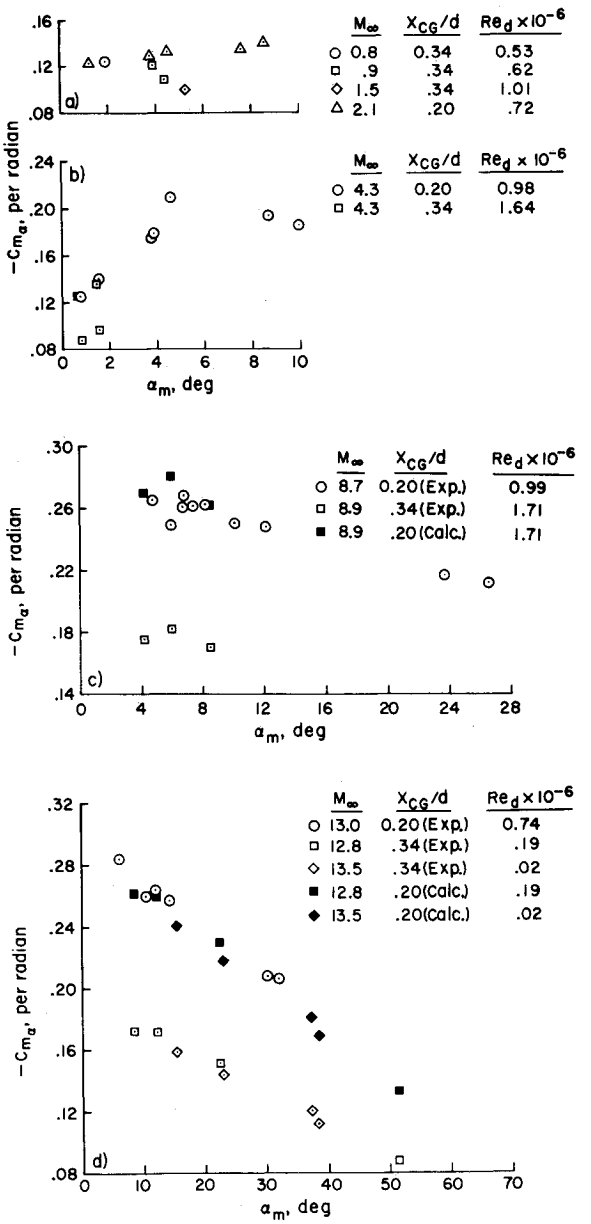

Fig. 5 Variation of static stability with pitch amplitude; a) $0.8 < M_\infty < 2.1$, b) $M_\infty \approx 4.3$, c) $M_\infty \approx 8.8$, and d) $M_\infty \approx 13$.

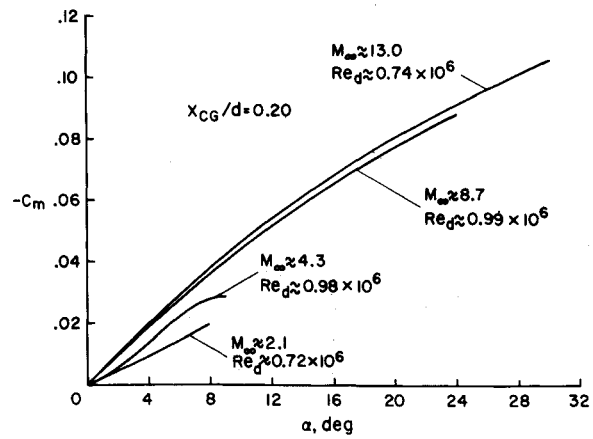

Fig. 6 Pitching-moment coefficient vs angle-of-attack.

However, this case depends heavily on one data point at an amplitude of 14° (Fig. 3d) and thus may not be well defined. Although the data are not conclusive, there appears to be an effect of Reynolds number over the broad range of these tests (0.005×10^6 to 0.74×10^6) such that the nonlinearities increase with decreasing Reynolds number. As a result, $C_{L_z}(\alpha = 0)$ decreases while $C_{L_z}(\alpha \gg 0)$ increases. Note that the difficulty of defining the lift curve increases in the very low Reynolds number range because of the decreased amplitude of the swerving motion.

Static and Dynamic Stability

The static stability data (C_{m_z}) and dynamic stability data ($C_{m_q}+C_{m_{\dot\alpha}}$) are presented in Figs. 5 and 8, respectively. Nonlinear pitching moments obtained from the static stability data by the method of Refs. 17 to 19 are presented in Fig. 6. Although these stability data are not critical to the reconstruction of the atmosphere, they are important in determining that the vehicle is properly aligned during entry and as the instrumentation sensors are deployed. Data for two different center-of-gravity locations are shown in Fig. 5. From the moment data of Fig. 6, the drag data of Fig. 2a, and the lift data of Fig. 4a, the center-of-pressure location of the model can be calculated. Results of these calculations, for two Mach numbers (Fig. 7), have been used to transfer the static-stability data of Figs. 5c and 5d to a common center of gravity. Note that the center-of-pressure location shown here is significantly forward of that shown in Ref. 6 for an identical forebody with no afterbody, which suggests that the afterbody significantly affects the normal force. This effect also may be seen in a comparison of lift-curve slopes for the complete PAET configuration and the forebody alone;[6] C_{L_z} is roughly 50% greater for the forebody than for the complete probe.

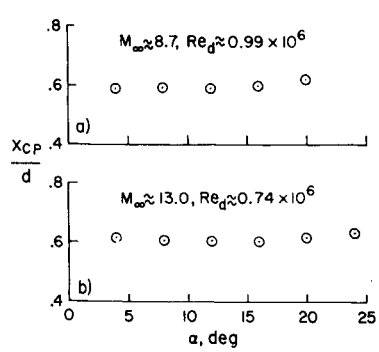

Fig. 7 Variation of center-of-pressure location with angle of attack; a) $M_\infty \approx 8.7$ and b) $M_\infty \approx 13$.

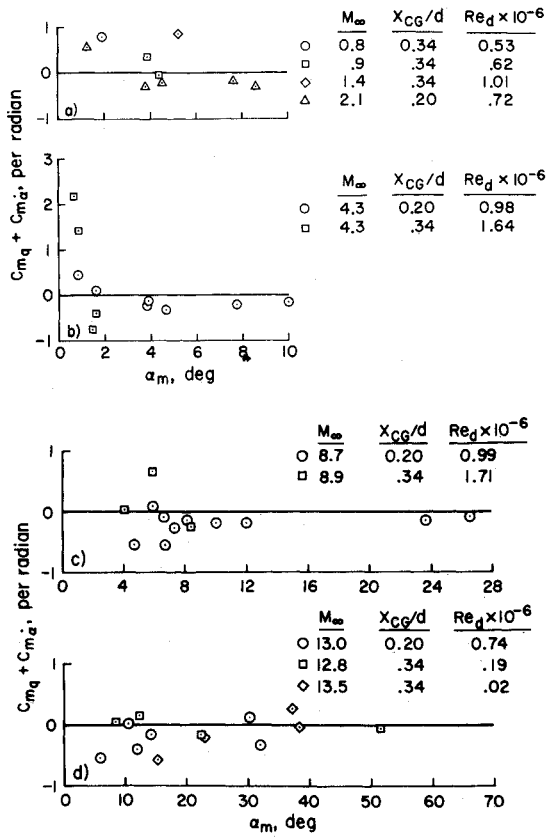

Fig. 8 Variation of damping-in-pitch derivative with pitch amplitude; a) $0.8 < M_\infty < 2.1$, b) $M_\infty \approx 4.3$, c) $M_\infty \approx 8.8$, and d) $M_\infty \approx 13$.

The model is, of course, statically stable for all the test conditions. However, different trends in the data are shown as a function of Mach number. At Mach numbers above 4.3, the static stability decreases with increasing pitch amplitude while at $M_\infty = 2.1$, C_{m_z} increases with increasing pitch amplitude. At an intermediate Mach number (4.3), C_{m_z} increases initially with amplitudes up to 5° but then decreases with a further increase in pitching amplitude. These trends are shown quite clearly in the pitching-moment curves in Fig. 6. There is no apparent explanation for the scatter in the aft center-of-gravity data in Fig. 5b. The static stability is not affected by Reynolds number in the range shown.

The data presented in Fig. 8 show that the PAET configuration is generally dynamically stable for $X_{cg} = 0.2d$ for all Mach

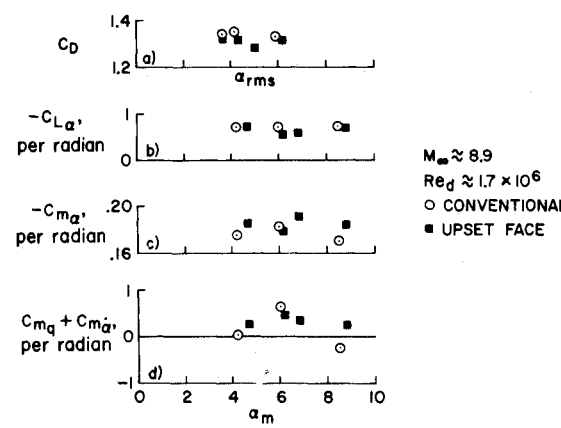

Fig. 9 Comparison at a Mach number of 9 of aerodynamic derivatives of the PAET configuration with conventional and upset face; a) drag, b) lift-curve slope C_{L_α}, c) static stability C_{m_z}, and d) damping-in-pitch derivative $C_{m_q}+C_{m_{\dot\alpha}}$.

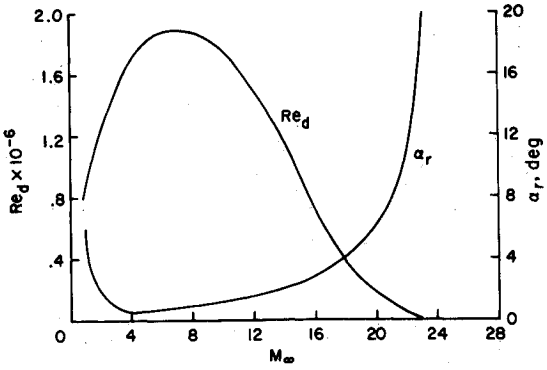

Fig. 10 Variation of Reynolds number and angle-of-attack with Mach number along the PAET entry trajectory.

numbers and pitching amplitudes greater than about 5°. (In the very low amplitude range, accuracy of the data is poor because of large relative measurement errors in angle-of-attack and sideslip.) These data show no consistent decrease in dynamic stability due to an aft center-of-gravity movement ($x/d = 0.20$ to 0.34) as would be expected from Ref. 7, where an aft movement of the center of gravity was found to be destabilizing. However, the present data are for differing Reynolds number and this fact may tend to mask any significant change due to the shift in the center-of-gravity location.

Concern that temperature or ablation could cause a discontinuity between the beryllium heat shield and the adjacent forebody and possibly trip the boundary layer led to the tests of the models incorporating an upset face. Comparison of the results of these tests with the basic data (Fig. 9) shows no appreciable effect of the discontinuity on the aerodynamic characteristics of the model except possibly in dynamic stability. Because the discontinuity tested was much greater than would be expected for the full-scale vehicle, it was concluded that any discontinuity actually experienced by the full-scale vehicle should have no significant effect on the aerodynamic characteristics.

Full-Scale Flight Data

On the day of the PAET entry, measurements of the Earth's atmosphere were made by means of Radiosondes (0–20 km alt), Arcasondes (20–55 km), and Viper Dart inflated spheres (>55 km). These measurements allowed the drag and static stability of the full-scale PAET vehicle to be derived from the on-board measurements of the aerodynamic accelerations in 3 coordinate axes. The drag coefficients and static stability measured from the flight data are compared with those from the ground facilities, ballistic range and wind-tunnels, insofar as possible, at the same Reynolds numbers, Mach numbers, and angles of attack as those experienced by the PAET vehicle along its entry trajectory. The flight variations of Reynolds number and angle of attack are shown in Fig. 10 as a function of Mach number.

Figure 11 presents the comparison of drag coefficients. Note that the accuracy of the full-scale flight data would be expected

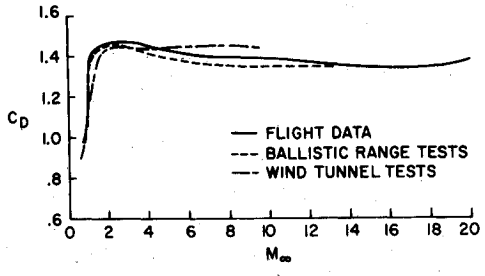

Fig. 11 Comparison of drag coefficient and Mach number obtained from flight and ground facilities.

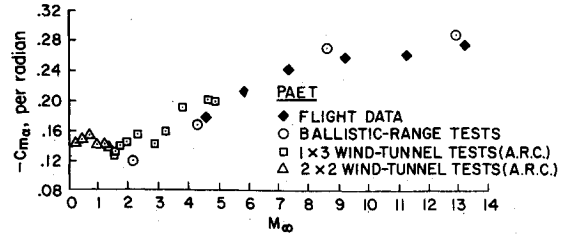

Fig. 12 Comparison of ground facility and flight data on the static-stability derivative (C_{m_α}).

to deteriorate at the higher altitudes (comparable to the higher Mach numbers) because of the difficulties involved in measuring the atmosphere with inflated spheres.[4] The agreement between the ground facility and flight data was nevertheless quite good, usually within 2 or 3%. For the wind tunnel data, the maximum disagreement with flight data varied from −18% at $M_\infty = 1$ to +4% at $M_\infty = 7.5$ (Refs. 8–15 and unpublished data from the Ames 1- by 3- and 2- by 2-ft Wind Tunnels). Results similar to this (at $M_\infty = 1$) were noted in Ref. 7. Although the reason for this difference is not conclusively identified, it is thought to be the result of sting and wall interference.

The quasilinear value of the static-stability derivative (C_{m_α}) of the entry vehicle determined from analyses[17] of the angular motion during entry also shows reasonably good agreement above a Mach number of 5 with data obtained in the ballistic range and in wind tunnels near zero angle of attack (Fig. 12). [The static-stability data from tests in the Ames 1- by 3- and 2- by 2-ft Wind Tunnels at angles of attack less than 1° are included in Fig. 12 because the angles of attack experienced in flight were small at the lower Mach numbers (see Fig. 10).] Flight data are not shown below $M_\infty = 4.7$ since the vehicle motion became somewhat erratic at this point,[4] undoubtedly due to effects of random aerodynamic disturbances and buffeting.

Conclusions

The test data reported here effectively "calibrated" the PAET flight experiment accurately so as to permit the generally excellent reconstruction of the atmosphere reported in Ref. 4. Of particular interest was the behavior of the drag coefficient at very low Reynolds numbers, down to 5000, which was needed near the threshold of the flight experiment. The drag coefficient was reduced by as much as 15% because of the reduced Reynolds number, when compared with more usual test conditions (Reynolds numbers on the order of 10^5 to 10^6).

The measured lift characteristics showed a large loss in lift-curve slope with increasing Mach number in the supersonic range. At hypersonic Mach numbers, nonlinearities became slightly more pronounced, and the effect of reducing Reynolds number was to increase the nonlinearity.

The test data showed that the models were statically and dynamically stable, becoming increasingly more stable (statically) with increasing Mach number. Only moderate nonlinearities were found. An interesting aspect was the comparison of center of pressure and lift-curve slope for the forebody alone[6] with that for the complete probe, which showed that the hemispherical afterbody significantly affected C_L, C_N, and the center-of-pressure position.

The comparison of the ground facility data, particularly these ballistic range data, with full-scale flight aerodynamic coefficients supports the validity of the ground facility tests. Accuracies in drag coefficient within 2 or 3% were indicated, and residual disagreements are probably largely due to uncertainties in ambient density at the flight altitudes. Comparisons of the flight data with transonic wind-tunnel data suggest that important wall and sting interference effects were present in the wind-tunnel tests, transonically. Comparisons of the static-stability coefficients for Mach numbers above 5 support the ground facility data within 5 to 10%.

References

[1] Seiff, A. and Reese, D. E., Jr., "Defining Mars' Atmosphere—a Goal for Early Missions," *Astronautics and Aeronautics*, Vol. 3, No. 2, Feb. 1965, pp. 16–21.

[2] Peterson, V. L., "A Technique for Determining Planetary Atmosphere Structures for Measured Accelerations of an Entry Vehicle," TN D-2669, 1965, NASA.

[3] Sommer, S. C., Boissevain, A. G., Yee, L., and Hedlund, R. C., "The Structure of an Atmosphere from On-Board Measurements of Pressure, Temperature, and Acceleration," TN D-3933, 1967, NASA.

[4] Seiff, A., Reese, D. E., Sommer, S. C., Kirk, D. B., Whiting, E. E., and Niemann, H. B., "PAET, an Entry Probe Experiment in the Earth's Atmosphere," *Icarus*, Vol. 18, No. 4, April 1973, pp. 525–563.

[5] DeRose, C. E., "Trim Attitude, Lift and Drag of the Apollo Command Module with Offset Center-of-Gravity Positions at Mach Numbers to 29," TN D-5276, 1969, NASA.

[6] Sammonds, R. I., "Aerodynamics of Mars Entry Probe-Lander Configurations at a Mach Number of 10," TN D-5608, 1970, NASA.

[7] Sammonds, R. I., "Dynamics of High-Drag Probe Shapes at Transonic Speeds," TN D-6489, 1971, NASA.

[8] Campbell, J. F., "Longitudinal Aerodynamic Characteristics of Several High-Drag Bodies at Mach Numbers from 1.50 to 4.63," TN D-3915, 1967, NASA.

[9] Campbell, J. F. and Howell, D. T., "Supersonic Aerodynamics of Large-Angle Cones," TN D-4719, 1968, NASA.

[10] Campbell, J. F., "Supersonic Aerodynamic Characteristics and Shock Standoff Distances for Large-Angle Cones with and without Cylindrical Afterbodies," TN D-5334, 1969, NASA.

[11] Campbell, J. F. and Howell, D. R., "Supersonic Lifting Capabilities of Large-Angle Cones," TN D-5499, 1969, NASA.

[12] South, J. C., Jr., "Calculation of Axisymmetric Supersonic Flow Past Blunt Bodies with Sonic Corners, Including a Program Description and Listing," TN D-4563, 1968, NASA.

[13] Nichols, J. and Nierengarten, E., "Static Aerodynamic Characteristics of Blunted Cones and Round-Shouldered Cylinders Suitable for Planetary Entry Vehicles at a Mach-Number Range 1.65 to 9.00," JPL WT20-558, 1964.

[14] Nichols, J. O. and Nierengarten, E. A., "Aerodynamic Characteristics of Blunt Bodies," JPL TR32-677, 1965.

[15] Walker, B. and Weaver, R. W., "Static Aerodynamic Characteristics of Blunted Cones in the Mach-Number Range from 2.2 to 9.5," JPL TR32-1213, 1967.

[16] Canning, T. N., Seiff, A., and James, C. S., eds., "Ballistic Range Technology," AGARDograph 138, Chap. 2, Aug. 1970.

[17] Malcolm, G. N. and Chapman, G. T., "A Computer Program for Systematically Analyzing Free-Flight Data to Determine the Aerodynamics of Axisymmetric Bodies," TN D-4766, 1968, NASA.

[18] Rasmussen, M. L. and Kirk, D. B., "On the Pitching and Yawing Motion of a Spinning Symmetric Missile Governed by an Arbitrary Nonlinear Restoring Moment," TN D-2135, 1964, NASA.

[19] Canning, T. N., Seiff, A., and James, C. S., eds., "Ballistic Range Technology," AGARDograph 138, Chap. 7, Aug. 1970.

JANUARY 1975 J. SPACECRAFT VOL. 12, NO. 1

Attitude Time-Series Estimator for Rectification of Spaceborne Imagery

R. H. CARON* AND K. W. SIMON†
TRW Systems Group, Redondo Beach, Calif.

Unprocessed digital multispectral imagery from the ERTS-1 satellite exhibits distortions due to fluctuations in the spacecraft's attitude. These distortions are easily removed if the attitude time-series of the spacecraft can be estimated with sufficient precision. A solution to this estimation problem is offered in the form of a discrete-time, sequential, mean-square-sense optimal estimator which uses ground control point observables. A computer implementation and performance evaluation using ERTS-1 data is discussed.

Nomenclature

ERTS	= Earth Resources Technology Satellite
MSS	= multispectral scanner
BIAT	= bulk image annotation tape
GCP	= ground control point (observation)
ICT	= image center time
ECR	= earth-centered rotating (coordinate system)
pixel	= picture element
$\mathbf{R}_G$	= ECR position of a GCP
$\Psi = (\Psi_r, \Psi_p, \Psi_y)$	= attitude time-series coefficient vector
$\sigma = (\mathbf{R}_S, \mathbf{V}_S)$	= ephemeris time-series vector
β	= mirror scan angle time-series
t	= time
ϕ	= MSS detector deployment angle
$\mathbf{n}$	= observation noise vector
$\theta = (\theta_r, \theta_p, \theta_y)$	= attitude time-series vector
δ	= distance between the spacecraft and a GCP
$\mathbf{u}$	= MSS unit scan vector in ECR
$\|\cdot\|$	= Euclidean norm
$\lvert\cdot\rvert$	= absolute value operator
R, P, Y	= local orbit-based coordinates
∇_q	$= \left[\frac{\partial}{\partial q_1}, \ldots, \frac{\partial}{\partial q_n}\right]^T$
	= matrix partial differentiation operator
$\lfloor x \rfloor$	= greatest integer not exceeding x
$\hat{\Psi}$	= estimator of Ψ
$A(k)$	= optimal gain matrix
$P(k)$	= estimator error covariance matrix
$\Lambda(k)$	= covariance matrix of $\mathbf{n}$
ε_p	= norm of the position estimation error
C	= cosine
S	= sine

Received May 22, 1974; revision received August 26, 1974. The authors are indebted to M. Byerly of the U.S. Geological Survey, who supplied the precision geodetic inputs necessary to evaluate the estimator, and B. Peavey of NASA/GSFC, who provided technical information relative to the ERTS-1 system.

Index categories: Computer Technology and Computer Simulation Techniques; Data Sensing and Presentation or Transmission Systems; Spacecraft Attitude Dynamics and Control.

* Member Technical Staff.
† Section Head.